Cooperativity between Integrin Activation and Mechanical Stress Leads to Integrin Clustering.

Olivier Ali, Hervé Guillou, Olivier Destaing, Corinne Albiges-Rizo, Marc R. Block, Bertrand Fourcade

Cooperativity between integrin activation and mechanical stress leads to integrin clustering

O. Ali,
H. Guillou$^\diamond$,
O. Destaing,
C. Albigès-Rizo,
M. R. Block,
and B. Fourcade[1]

April 6, 2011

[1]Corresponding author. Address: INSERM U823 - CNRS ERL-5284 Équipe Dysad, Institut Albert Bonniot, Site Santé La Tronche, Grenoble, BP170 Grenoble Cédex, France, Tel.: (33)6 82 17 37 29, Fax: (33)4 76 54 94 65, Bertrand.Fourcade@ujf-grenoble.fr

Abstract

Integrins are transmembrane receptors involved in crucial cellular biological functions such as migration, adhesion and spreading. Upon the modulation of integrin affinity towards their extracellular ligands by cytoplasmic proteins (inside-out signaling) these receptors bind to their ligands and cluster into nascent adhesions. This clustering results in the increase in the mechanical linkage between the cell and substratum, cytoskeleton rearrangements, and further outside-in signaling. Based on experimental observations of the distribution of focal adhesions in cells attached to micro-patterned surfaces, we introduce a physical model relying on experimental numerical constants determined in the literature. In this model, allosteric integrin activation works in synergy with the stress build by adhesion and the membrane rigidity to allow the clustering to nascent adhesions independently of actin but dependent on the integrin diffusion onto adhesive surfaces. The initial clustering could provide a template to the mature adhesive structures. Predictions of our model for the organization of focal adhesions are discussed in comparison with experiments using adhesive protein microarrays.

Keywords: Integrin, Activation, Clustering, Mechanotransduction, Nano-patterning, Mathematical Modeling.

Introduction

Integrins(1) are allosteric transmembrane adhesive proteins with a key role in cell-substrate adhesion and in mechanotransduction, a process by which mechanical forces are transducted into biochemical signals(2). This inside-outside signaling relies on intracellular soluble factors such as talin able to bind to the integrin cytoplasmic tail(3–5). They induce a conformational change from an inactivated to an activated state with an increase in affinity for the extracellular matrix(6). A general property of all adhesive structures - in their nascent, focal or fibrillar states - is the recruitment and the clustering of integrins together with compositional changes depending on their maturation stage. Understanding the coupling between integrin activation and integrin clustering is of crucial importance, since integrin activation and clustering regulate cell adhesion and migration through mechanotransduction.

In this paper, we focus on the physical mechanisms that regulate lateral assembly of integrins, i.e. initial clustering, in the absence of F-actin(7) but that are talin dependent. Talin binding mediated activation of integrins is β subunit specific and occurs with a weak affinity(8–10). In this limit, we show that integrin activation and integrin clustering can be described within the same inside-outside signaling framework. The essential ingredient of our model is the switch between the two integrin affinity states when this switch is induced by a diffusible factor. Previous work(11) has shown that talin binding in the absence of force or other proteins is sufficient to induce the activated form of integrin. To this end, we develop an elementary mechanotransduction model based on an activator field to mimic the role of talin regulating integrin binding to the extracellular matrix. Due the competition between the stress and the allosteric activation, talin concentration is increased by diffusion on stressed integrins. This, in turn, provides a robust mechanism for integrin clustering into stationary structures. The existence of such clusters can be experimentally tested by modifying the elementary molecular modules for integrins activation and adhesion(12). As a result, we show that affinity regulation can induce by itself the clustering in nascent adhesion complexes that provide the template of mature focal adhesion patterns(7, 13). The principal result reported in this paper is that neither direct nor indirect interaction with actin cytoskeleton is necessary to trigger the initial clustering which results only from the activation field sensed by the stressed integrins.

By comparison, former theoretical works have already emphasized the role of acto-myosin mechanical forces for the maturation focal adhesions(14). Stress-sensing models such as the clutch model studied in (15), anisotropic growth of focal adhesions in the direction of the applied force(16, 17), force-induced recruitment of integrin partners (18), or integrin redistribution caused by substrate rigidity have already been modelized(19). The present work introduces however, a new mechanotransduction model which should be valid for nascent focal adhesions and which does not require the acto-myosin activity but only talin binding to integrins.

To make connections with experimental studies, we include in this paper experimental results for cells adhering on adhesive protein microarrays. In the last section, our model will be discussed in the light of these experimental findings by predicting different geometries integrin clusters depending on the size of the adhesive spots.

Methods

Materials

Alexa 488-, 546-, and 633-conjugated secondary antibodies were from Invitrogen Carlsbad, CA. TRITC conjugated phalloïdin and Pluronic F127^{TM} is from Sigma Aldrich (l'isle d'Abeau, France).

Cell culture

NIH 3T3 fibroblasts were cultured in α-MEM (Gibco-InVitrogen, Oxon, UK) supplemented with 10% inactivated fetal calf serum, penicillin and streptomycin and were harvested with trypsin/EDTA. Cells were plated with 60,000 cells in 2 ml on micro structured arrays (area of 440 mm^2) in 30-mm Petri dishes and were left to spread for 4 h.

Micro-patterning and functionalization

Patterned protein glass cover slips were performed according to (20) with slight modifications. Glass cover slips (22 × 22 mm) were washed in a solution of sulfuric acid and hydrogen peroxide (7:3, vol:vol) for 30 min, dried,

and then dipped for 1 h in a solution of octadecyltrimethoxysilane and amino-propyltrimethoxy silane (3:1, mol:mol) (Sigma-Aldrich) in toluene. Positive photoresist resin (Shipley, S1805, Rhom & Haas Electronic Materials, Villeur-bane, France) was spin-coated and cured according to the manufacturer's protocol to form a uniform, UV-sensitive film 0.5-?m thick. The coated cover slips were then insolated with UV light using a Karl Süss aligner (MJB3, SUSS MicroTec, Saint-Jeoire, France) at 436 nm and 15 mJ/cm2 through a chromium mask. The irradiated pattern was revealed with microposit developer concentrate in deionized water (1:1, vol:vol) (Shipley, MF CD-26, Rhom & Haas Electronic Materials). The patterned cover slips were incubated for 1 h at 37°C in a solution of gelatin-RITC and 10 μg/ml vitronectin in phosphate-buffered saline (PBS). Substrates were rinsed in PBS and then in absolute ethanol in an ultrasonic water bath to dissolve the photoresist resin. Finally, either antiadhesive triblock copolymer Pluronic F127^{TM} at a concentration of 4% in water for 1 h 30 min at 37°C, or a solution of FN7–10-FITC (Fibronectin type 1II domains 7-10 conjugated to FITC) at 5-15 $\mu g/ml$ in PBS was adsorbed to the complementary pattern revealed after resin dissolution by ethanol for 1 hour at 37°C. Following a last rinse in PBS, 155 cells/mm^2 were seeded and incubated overnight, prior to fixation and staining.

Results

Cell were spread on protein microarrays with adhesive spots of either $4 \times 4\,\mu m$ or $2 \times 2\,\mu m$ made of the fibronectin cellular attachment domain (FN 7-10) and separated by anti adhesive surfaces of polyethylene oxide as described in the supplemental section. On these surfaces, the final shape of spread cells is not predetermined since the cells can use one adhesive spot or another. Indeed, when the lateral distance between two consecutive islands was no more than $8\,\mu m$, NIH 3T3 cells attached and spread on the array in a manner similar to that usually observed on uniformly coated surfaces (not shown), whereas when the distance between adhesive islands increased up to $16\,\mu m$, most of the cells adopted simplified shapes corresponding to thermodynamic metastable states(21). Vinculin staining of focal adhesions that are sustained by integrin clusters revealed that only external adhesive islands where used as attachment sites. This is due to pattern symmetries which imply that the resulting force applied by the stress fibers on an internal adhesive island
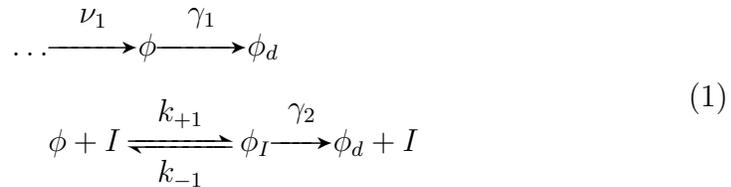
is zero. Therefore, the lack of mechanical cues did not allow focal adhesion assembly on these spots. On $4 \times 4\,\mu m$ adhesive islands with $16\,\mu m$ spacing (Figure 1, left panels), however, one could always detect two focal adhesions by adhesive island even when the cells were only using two fibronectin spots. This latter result clearly demonstrates that tensions along actin stress fibers connected to focal adhesions are not the driving forces for integrin clustering. Surprisingly, when the dimensions of the adhesive plots were reduced to $2 \times 2\,\mu m$, a single integrin clustering connected to fuzzier actin stress fibers was observed on external adhesive islands (Figure 1, right panels). Even in the angles where orthogonal forces occurred, a single focal adhesion was detected. These experimental data indicated that beside the tensions that promote focal adhesion growth, an additional mechanism is required to explain the splitting of adhesive clusters at constant tension.

Discussion and theory

Preliminaries

For what follows, it will be useful to consider the cycle of elementary reactions for talin as shown in Figure 2. In the cytosol, talin is in the inactivated state with concentration ϕ_c. When adsorbed on the membrane, talin changes conformation and is activated by binding to PiP_2(22). Once activated, talin diffuses on the membrane and interacts with integrin receptors under the control of other proteins such as RIAM(5) and kindlins(23). Finally, downstream of integrin activation, talin ubiquitination and degradation leads to disassembly of adhesive clusters(24). In particular, as shown in Ref. (24), increasing the rate of talin degradation by increasing the affinity of talin to ubiquitin ligase Smurf1 not only increases the turnover of focal adhesions but, additionally, increases noticeably their number and their size (see Fig. 3 in (24)). This indicates that talin degradation may also be involved at the early stages of nascent adhesions and focal adhesion maturation processes.

Overall, the cycle can be represented as follows

$$\ldots \xrightarrow{\nu_1} \phi \xrightarrow{\gamma_1} \phi_d$$

$$\phi + I \underset{k_{-1}}{\overset{k_{+1}}{\rightleftharpoons}} \phi_I \xrightarrow{\gamma_2} \phi_d + I \tag{1}$$

where talin is activated at a rate ν_1 with concentration ϕ and can reversibly bind to an integrin I with rate constants $k_{\pm 1}$. Membrane bound talin is also irreversibly inactivated at a rate γ_1. Finally, γ_2 is an irreversible dissociation rate and simulates adhesion complex disassembly by degradation.

Table 1 gives the order of magnitude of key physical constants used in our model. Among them, the life time $1/b \simeq 100\,s$ of talin in its activated state gives a characteristic diffusion length $\lambda = \sqrt{D_\phi/b} \simeq 2 - 4\,\mu m$. This characteristic length is comparable to critical size w_c of the adhesive spots above which the focal adhesion clusters split into two clusters. Henceforth, the ratio of the diffusion length, λ, to the spot size, w_0, will play a key role in determining different families of solutions for integrin clustering.

In general, the concentrations depend both on space coordinates $\mathbf{x}$ and on time t. If $\mathbf{x}$ is taken along the cell adhesive substrate, $\phi(\mathbf{x}, \mathbf{t})$ is the surface concentration of talin in the activated state and $\phi_I(\mathbf{x}, \mathbf{t})$ the average number of talin per integrin. If $n_0(\mathbf{x}, \mathbf{t})$ is the total concentration of integrins, $n_0\phi_I$ is the concentration per unit of surface of talin-integrin complexes. We will refer to this state as the adsorbed phase.

In what follows, we will work in the quasi-steady state approximation where ϕ_I is in equilibrium with the local concentration of talin $\phi(x, t)$. When talin is bound to an engaged integrin, it cannot diffuse and local equilibrium fixes an algebraic condition between $\phi(\mathbf{x})$ and ϕ_I. This relationship is found from the last step of Eq. (1) and reads as

$$\phi_I = \phi/(\phi + K_m) \text{ with } K_m = \frac{k_{-1} + \gamma_2}{k_{+1}} \simeq \frac{\gamma_2}{k_{+1}} \qquad (2)$$

where K_m is a Michaelis-Menten constant with the dimension of a concentration. The last approximation points out the importance of two pathways for talin unbinding, one of which being stress sensitive. Typically, the dissociation rate k_{-1} is of the order of $7.4\,10^{-4}s^{-1}$ (25) and if γ_2 is of the same order of $b \simeq 10^{-2}s^{-1}$, the variations of K_m with k_{-1} can be neglected. Thus, K_m is independent of the strain which influences the off-rate of talin unbinding. Using $k_{+1} \simeq 10^3 l \cdot Mol^{-1}$ (25), we find $K_m = 10^{3-4}$ molecules per μm^2.

Two limit cases will be of interest. For small concentrations ϕ, ϕ_I is simply proportional to ϕ. In the saturated limit, however, ϕ_I is independent

of ϕ and approaches unity. To summarize for later use, we have :

$$\phi_I \simeq \phi/K_m \quad \text{when } \phi \ll K_m \tag{3}$$

$$\phi_I \simeq 1 \qquad \text{when } \phi \gg K_m \tag{4}$$

Other non-linearities with $\phi_I = a\phi^\gamma/(1+\phi^m)$ where a, γ, m positive numbers can be included in the model without qualitative changes.

Model for integrin activation and engagement

Step (3) of Fig. 2 corresponds to the reversible binding of talin to integrin. In our model, these kinetic rate constants are determined by talin allosteric activation of integrins and by elasticity.

We recall that talin binding to an integrin induces a conformational change for the integrin receptor proteins. According to (10), the integrin extracellular domain is in its extended conformation in the activated state with talin bound to the intracellular tail. In this state, an integrin is bound to its ligand. By contrast, in the other state, the head is in the bend conformation. In this unactivated state, the integrin has a smaller probability to bind to its ligand. Henceforth, we will consider the very large affinity limit for extracellular ligand binding where an activated integrin is engaged, whereas an unactivated one is free to diffuse. To summarize, binding talin to an integrin introduces a conformational change between two states with respective density $n_{u,b}$, where the density of integrin is conserved $n_u + n_b = n_0$.

Local equilibrium between these two states is always achieved at a time scale much smaller than the typical time scale for concentration changes due to diffusion. Let $K_e(\phi_I, h)$ be the effective equilibrium constant for integrin engagement. $K_e(\phi_I, h)$ depends both on the adsorbed talin field $\phi_I(\mathbf{x}, t)$ and on a strain field $h(\mathbf{x})$ and local equilibrium implies that the density of bound integrins obeys

$$n_b(\phi, h) = \frac{n_0}{1 + K_e(\phi_I, h)^{-1}} \tag{5}$$

All together $\phi_I(\mathbf{x}, t)$ and $h(\mathbf{x})$ play antagonistic roles for adhesion when the concentration of talin $\phi(x)$ is homogeneous. On the one side, binding talin favors adhesion and thus increases the affinity constant for the extracellular matrix. On the other side, stretching the integrin extracellular head with a length $l(\mathbf{x})$ that differs from a reference length $l_0 \simeq 10\,nm$ induces a stretching energy $\frac{1}{2}k_b h(\mathbf{x})^2$ with $h(\mathbf{x}) = l(\mathbf{x}) - l_0$. By definition, k_b is an effective

rigidity constant which includes substrate deformability. Following Bell(26) and other(27, 28), this energy is of the order of few $k_B T \simeq 4\,pN.nM$ and adds up to the bare energy difference $\Delta f_{u,b}$ between the two integrin states. This regime is only valid for l smaller than a maximum extension ($\simeq 25\,nm$) and we will henceforth restrict ourselves to this range.

Since binding talin decreases the free energy of the activated state, we have $\Delta f_{u,b} = -A_I \phi_I$ where $-A_I$ is the interaction energy between talin and the cytoplasmic β-subunit. In the zero stress limit where $\phi_I = \phi_I^0$, we have $A_I \phi_I^0 \simeq 2.5\,k_B T$(9, 29). Summing the allosteric and the elastic contributions gives the enthalpy difference between the two states

$$\Delta H_{u,b} = \Delta f_{u,b} + \frac{1}{2} k_b h(\mathbf{x})^2 \tag{6}$$

Using Van't Hoff law, the equilibrium constant follows

$$K_e(\phi_I, h) = K_{e,0} e^{-\beta\left(\frac{1}{2} k_b h(\mathbf{x})^2 - A_I \phi_I\right)} \tag{7}$$

where $K_e^0 = K_{e,0} \exp\left(A_I \phi_I^0\right)$ is the equilibrium constant in the absence of stress. This state is a reference state and the principle of the model is to perturb this reference state by strain elasticity with $h(x) > 0$. K_e^0 fixes the number of bound integrins by Eq. (5) and is thus a small number ($K_e^0 = 10^{-3}$ in this work).

To comment Eq. (7) further, we note that NMR studies as in Ref. (10) indicate that the interaction between the two different talin isoforms and the membrane-proximal domain of an integrin is specific of the integrin species. In parallel, small variations of the talin-integrin interaction A_I lead to very different values of the equilibrium constant (7) when the talin concentration varies. This, in turn, will demonstrate that integrin clustering behavior is specific of the integrin family.

Integrin engagement is stress dependent

In our model, allosteric activation and tail elasticity contribute to the chemical potential $\mu(\phi_I, h)$ per integrin. This chemical potential will influence the desorption rate k_{-1} in Eq. (1) and, thus, will modify the equation of motion for talin diffusing on the membrane. To compute the chemical potential, we

neglect all entropic contributions and retain the most singular part as

$$\mu(\phi_I, h) \simeq \frac{\delta}{\delta\phi_I} \left[\frac{1}{2} n_b(\phi_I, h(\mathbf{x})) k_b h(\mathbf{x})^2 \right]\Bigg|_{g_I(\phi,\phi_I)=0} \tag{8}$$

which follows from Eq. (6) times the probability density to find an integrin in its activated-engaged state. From Eq. (5), $n_b(\phi_I, h)$ is step like when ϕ varies at constant strain $h(x) = h_0$. Taking the derivative as done in Eq. (8) introduces a delta-like singularity in the chemical potential when talin allosteric activation compensates strain elasticity

$$A_I\phi_I = \frac{1}{2}k_b h_0^2 - \frac{1}{\beta}\ln(K_e^0) \tag{9}$$

which is approximately equal to $10k_BT$ for $h_0 = 5 - 10\,nm$.

Since the chemical potential depends on the strain $h(x)$ by Eq. (8), varying $h(x)$ influences integrin engagement and talin concentration. Experimentally, $h(x)$ can be varied in numerous ways. For example, the use of micro-patterned substrates concentrates the stress at the margin of the adhesive spots. An other way is to probe directly $h(x)$ using single molecule assays to stretch the integrin head in the nm range.

Henceforth, we will work in the thermodynamic ensemble where the strain is fixed at a given function $h(x)$. For numerical and analytical convenience, $h(x)$ will be taken as a gaussian $h_0 \exp\left(-x^2/2w_0^2\right)$ of width w_0 and height h_0. As shown below, the state of the system is globally independent of exact analytical form of $h(x)$ as long as $h(x)$ can be greater than some threshold value on a region of size w_0 larger than the diffusion length $\sqrt{D/b}$.

Talin equation of motion

Step 3 of Fig. 2 is the adsorption-desorption process for the dynamic of the activated talin $\phi(\mathbf{x})$ which is otherwise allowed to diffuse on the membrane with diffusion constant D_ϕ. The chemical potential of Eq. (6) influences the desorption rate of talin-integrin bound state to the free state. At the end, the theory is self-consistent, since this desorption rate for talin-integrin unbinding depends on the local concentration ϕ.

To derive this self-consistent equation, we define a reference state concentration ϕ_0 of talin at zero stress ($h(\mathbf{x}) = 0$, see Appendix A). When measured

with respect to this reference state, $\phi \rightarrow \phi + \phi_0$, the equation of evolution for the relative excess of concentration ϕ is written as

$$\partial_t \phi = D_\phi \Delta \phi - b\phi + \frac{1}{2}\Gamma_I k_b h^2 \frac{\partial n_b}{\partial \phi_I}\bigg|_{g(\phi,\phi_I)=0} \tag{10}$$

where the last term is proportional to the excess of chemical potential in the bound phase due to strain elasticity. Physically, this term describes how an excess of talin compensates for the increase of the desorption rate due to integrin engagement. Using the model of Eq. (1), this equation is derived in Appendix A under the assumption that the kinetic rate constant for talin desorption is influenced by the chemical potential of Eq. (8) which contains stress elasticity. The diffusion-reaction equation (10) is thus equivalent to the one used to study the growth of focal adhesions(18), but with a talin dependent strain elasticity.

In Eq. (10), Γ_I is a kinetic coefficient between the talin bound and free states and is proportional to the off-rate of the talin-integrin unbinding. Since Γ_I is proportional to A_I, Γ_I reflects the talin affinity for an integrin, Γ_I is also β-subunit specific. The last term is proportional to the density n_0 of integrins. As the bare affinity K_e^0 is small, $n_b(\phi_I, h)$ is a step function when ϕ_I varies. Thus, $\partial n_b / \partial \phi_I$ has a singularity to mimic the switch in integrin affinity toward its ligand(30). This term depends on ϕ by the quasi-steady state condition $g_I(\phi, \phi_I) = 0$. Thus the dynamic of the field $\phi(\mathbf{x})$ depends on diffusion by D_ϕ, on the residence time of talin in its activated state by b and, finally, on the strain $h(\mathbf{x})$. This equation describes how elasticity provides a positive feedback loop for integrin activation when the source term in (10) is maximum.

Integrin equation of motion

Eq. (10) gives the correct evolution of $\phi(\mathbf{x})$ as long as the integrin density $n_0(\mathbf{x})$ does not respond to the variations of $\phi(\mathbf{x})$. Since the integrin diffusion constant is smaller than the one for talin, this approximation holds at very short times. At longer times, however, there is a change in integrin concentration $n_0 = n_u + n_b$, since unbound integrins n_u diffuse (diffusion constant D_n). Because of local equilibrium, the equilibrium constant gives the fraction

of bound to unbound integrins as

$$\frac{n_b(\mathbf{x}, t)}{n_u(\mathbf{x}, t)} = K_e(\phi_I, h) \tag{11}$$

As a result, the effective diffusion equation for the integrin concentration field $n_0(\mathbf{x}, \mathbf{t})$ reads as

$$\frac{\partial n_0}{\partial t} = D_n \Delta \left[\frac{n_0}{1 + K_e(\phi_I, h)} \right] \tag{12}$$

Eq. (12) together with Eq. (10) gives a complete system for a given strain profile $h(\mathbf{x})$.

Effective diffusion-reaction equation

The essential property of our model is that its describes integrin activation in cooperation with changes in talin concentration. From now on, we will concentrate in the small talin concentration limit with $\phi_I = \phi$, see Eq. (3). The large ϕ limit of Eq. (4) where ϕ_I saturates is studied in the last section. Mathematical analysis will focus on the one-dimensional case when the typical radius of curvature of the adhesive spot is larger than de diffusion length $\sqrt{D/b}$.

Using the two equations of motion, we solve the problem as follows. In the symmetric case $h(\mathbf{x}) = h(-\mathbf{x})$, Eq. (12) has the unique solution

$$n_0(x, t) = \frac{n_\infty}{1 + K_e^0} \left[1 + K_e(\phi_I, h) \right] \tag{13}$$

Since Eq. (10) is valid for an arbitrary integrin density n_0, we use (13) in Eq. (10). As a result, we solve the effective reaction-diffusion equation

$$\frac{\partial \phi}{\partial t} = D_\phi \Delta \phi + f(\phi, h) \tag{14}$$

with the source function $f(\phi, h)$

$$f(\phi, h) = -b\phi + \frac{1}{2} k_b h(\mathbf{x})^2 \frac{\Gamma_I}{1 + K_e^0} \frac{n_\infty}{1 + K_e(\phi_I, h)^{-1}} \Bigg|_{\phi_I = \phi/K_m} \tag{15}$$

In order to mimic adhesive spots surrounded by non-adhesive islands, boundary conditions are chosen so that both the strain $h(\mathbf{x})$ and the concentration $\phi(\mathbf{x})$ vanish at infinity.

The characteristic shapes of $f(\phi, h)$ are given in Fig. 3 in the small and large $h(\mathbf{x}) = h_0$ limits. For $h_0 < h_{c_1}$, $f(\phi, h(\mathbf{x}))$, has only one zero whereas, for $h_0 > h_{c_1}$, it has three zeros $\phi_{1,2,3}$. In that case, the system is again bistable. Thus, for an homogeneous strain profile $h(\mathbf{x}) = h_0 > h_{c_1}$, the effective diffusion equation can be used to describe lateral excitation of a signal which propagates with a threshold response. The existence of three zeros for the source functions $f(\phi, h)$ at fixed $h = h_0$ is a characteristic property of reaction-diffusion systems with propagating wave solutions. Henceforth, we will study stationary solutions of (14) with $\partial\phi/\partial t = 0$. These solutions may be seen as waves pinned by strain elasticity, since they are concentrated where the stress is maximum.

Integrin Clustering is stress dependent and is characterized by two families of solutions

In the allosteric model for integrin activation of Eq. (6), the elastic stress competes with the talin field to regulate integrin activation and engagement. When activated talin diffuses on the membrane, however, this competition leads on an amplification loop. To bias this competition, we vary the strain profile by changing h_0 and compute the stationary solutions for $\phi(x)$ and $n_b(x)$. Stability of these solutions with respect to variations in integrin concentration is checked using the equivalent equations (10) and (12) for different initial conditions in the regime where $\phi_3^\star$ in Fig. 3 tends smoothly to zero when x goes to infinity. Other strain functions $h(x)$ with characteristic variations on a width w_0 have been tested without qualitative changes. Solving the model amounts to comparing numerical solutions with asymptotic results as done in the next section.

Small stress regime $\phi_I \simeq \phi/K_m$: Numerical results

Fig. 4-a,b,c for the talin and integrin concentration fields demonstrate that stress leads to integrin clustering. Depending on the strain, this clustering is described by two families of solutions.

    1. For small stress values, $h < h_{c_1}$, clustering corresponds to a unique

centered distribution of ϕ which increases rapidly with h_0. These solutions correspond to the long dashed curves shown in the figure and they will be compared to the analytical solution in the next section. Type 1 solutions are always characterized by a centered maximum of talin concentration at the origin The distribution of bound integrins follows from the solution of $\phi(x)$ since :

$$\frac{n_b}{n_\infty} = \frac{K_e(\phi, h)}{1 + K_e^0} \tag{16}$$

where n_∞ is fixed by the condition at infinity. Type 1 solutions for n_b are characterized by a maximum at the origin. Only near bifurcation points, type 1 solutions for n_b may exhibit a local minimum.

2. At larger strain, $h > h_{c_1}$ where the source function (15) possesses three zeros, there is a new family of solutions. Type 2 solutions are characterized by a distribution of talin with a double symmetric maximum. These maxima merge with the centered maximum of type 1 solution when $h = h_{c_1}$. Using (16), the distribution of bound integrins is always symmetric with respect to the origin and concentrates rapidly at the margin of the zone where the stress is applied when h_0 is increased above h_{c_1}. Type 1 and 2 solutions exist for $h > h_{c_1}$ if the diffusion length is small enough with respect to the characteristic width w_0 of the strain $h(x)$, $D/bw_0^2 \ll 1$. They are both stable for a large class of initial conditions (using (10) and (12)).

Small stress regime $\phi_I \simeq \phi/K_m$: Analytical results

To get insights into the two families of stationary solutions, we approximate the source function $f(\phi, h)$ by its $\beta \to \infty$ limit. In this case, the Bolzmann function converges to the Heaveside $\theta[x]$ function with two inclines (see red curve of Fig. 3). The source function in Eq. (15) becomes

$$f_\triangle(\phi, h) = - b\phi + \frac{1}{2}\frac{\Gamma_I}{1 + K_e^0}n_\infty k_b h\left(\mathbf{x}\right)^2 \theta\left[A_I \phi/K_m - 1/2 k_b h(\mathbf{x})^2 + 1/\beta \ln K_e^0\right] \tag{17}$$

We call this model the β_∞ model and solve exactly for $\phi(x)$ as done in the supplemental data section. From this solution, we find $n_0(x)$ and $n_b(x)$ using

Eqs. (11) and (13). Plots of solutions of this asymptotic model are also given in Fig. 4-a,b for comparison with numerical data.

Type 1 solutions

Fig. 4-a corresponds to this case. This solution has a maximum (Eq. (**??**) of the supplemental data section). In the small diffusion length limit D/bw_0^2, we find (see thin curve in Fig. 4-a)

$$\phi_1(x=0) \simeq \frac{1}{2} k_b h_0^2 \frac{\Gamma_I n_\infty}{b(1+K_e^0)} \tag{18}$$

As expected, the concentration of talin increases with rigidity. Decreasing b, or equivalently increasing the life time of activated talin, has the same effect. From this, we find that the density of bound integrins for type 1 solution is asymptotically given by

$$\frac{n_{b,1}(x=0)}{n_\infty} \simeq K_e^0 \exp\left(\frac{1}{2}\beta k_b h_0^2 \left[\frac{A_I \Gamma_I n_\infty}{b K_m (1+K_e^0)}\right]\right) \tag{19}$$

What the model predicts is thus a local increase of ϕ, and therefore of ϕ_I, to counterbalance the negative effect of the strain h_0 on integrin engagement. Because of the exponential dependence, Eq. (19) is very sensitive to variations in strain h_0 and to changes in parameters. If the talin-integrin interaction energy A_I is multiplied by a factor 2, Γ_I changes by a factor of 4 and the exponential in (19) is raised to the same power. Such a sudden increase in integrin density upon small changes in A_I is the distinctive mark of a positive feedback loop contained in the model.

Type 2 solutions

In contrast to type 1 solutions, solutions of type 2 are characterized by a minimum of talin concentration at the origin. The width of this depletion zone is set by the diffusion length λ with $\phi(x) \propto \cosh(x/\lambda)$. Thus, for type 2 solutions, the effect of the strain is to exclude talin proteins from the center with a maximum of concentration at a characteristic distance $\pm w_0$. The calculation reported in the supplemental data section demonstrates that type 2 solutions cannot be constructed if the ratio λ/w_0 is to small. In this regime, diffusion smoothes out any irregularity in the strain profile $h(x)$

and, by symmetry, the concentration field of talin can only have a centered maximum.

Fig. 5-a shows how the distribution of talin evolves when w_0 decreases at fixed strain h_0. Starting at large width w_0, the distribution shrinks and the minimum is less pronounced as diffusion is more and more effective. At a critical width w_c, the two maxima merge at the origin. Below w_c, the unique solution is of type 1 with a centered maximum. Fig. 5-b is the accompanying figure for the distribution of bound integrins. Although the distribution of talin is centered below the bifurcation point, the distribution $n_b(x)$ may have a minima in its immediate vicinity.

The condition for existence of type 2 solution of the supplemental data section is given by the matching conditions of the two branches below and above the singularity given by the θ function in Eq. (17) when $\phi_2(x)$ satisfies condition (9). These conditions result from conservation laws which imply that concentration and current are conserved quantities when $\phi(x)$ passes through the singularity at $x = x_0$. For all curves of Fig. 4-b, this point is indicated by a dot. At bifurcation, this point coincides with the origine. From this, we compute the critical width w_c at given h_0 (see Eq. (**??**) with $x_0 = 0$)

$$\frac{\lambda^2}{\omega_c^2} = \frac{1}{2} k_b \frac{\Gamma_I A_I}{b(1 + K_e^0)} \frac{n_\infty}{K_m} \left(1 - 2 \frac{\ln K_e^0}{\beta k_b h_0^2}\right) \tag{20}$$

As a result, the critical width decreases with A_I and with the strain h_0. Using Table 1, Fig. 5-a gives a value for w_c of the order of 2-3 μm.

Eq. (20) is derived for a gaussian profile $h(x) = h_0 \exp\left[-x^2/(2w_0^2)\right]$. Numerical experiments with other strain profiles show small changes in the critical width w_c for different strain functions $h(x)$. A reason for this is that the source function (17) is independent of the strain profile near the origin, so that the $\cosh(x/\lambda)$ solution is universal and independent of the profile $h(x)$.

Large stress regime : Extension of the linear model to include the saturation limit of the bound talin field ϕ_I

Clearly, the linear regime $\phi_I = \phi/K_m$ is only valid at small strain h_0 and ϕ_I must saturate above a critical value fixed by the equivalent Michaelis-Menten constant as in Eq. (4). Since ϕ increases with h_0, see Eq. (18) for type 1 solutions, the boundary value ϕ above which the linear regime breaks down sets an equivalent condition for h_0.

In this saturated limit where ϕ_I tends to 1, the equilibrium concentration of talin bound to integrin is independent of ϕ, since all integrins are already activated. In that case, the equivalent source function for reaction-diffusion has only one fixed point instead of being tooth shaped as in Fig.3. Let us call h_{c_2}, the value of h_0 above which the equivalent source function $f(\phi, h_0)$ has only one zero. For $h_0 > h_{c_2}$, type 1 solutions cease to exist. Numerically, adding Langevin noise to the equation of motion or steric repulsion between integrins leads to the same effect when $n_0(x)$ is large since the saturated limit for type 1 solutions is very sensitive to fluctuations in integrin density.

Discussion and conclusion

To conclude, our approach leads to integrin clustering and embodies collective effects between different families of integrins. Thermodynamic provides an effective activation potential so that there is no need for direct or indirect interactions between the integrin receptors for clustering. The model can be represented as an effective reaction-diffusion system with the conclusion that integrin clustering is driven by integrin activation imposed by mechanical constraints. Mixing elasticity and chemical reactions reproduces the characteristic properties of excitable media which has already been evoked in the biological literature for the mechanical activation of Src(31).

Activation mediated by talin binding depends on the β integrin cytoplasmic subunits and this dependence is explicit in the model through the interaction energy parameter A_I. Small variations of this parameter lead to exponential variations of talin concentration and influences markedly the locus of bifurcation lines. Testing the role of $\alpha_5\beta_1$ and $\alpha_v\beta_3$ integrins for mechanotransduction has already be proposed in recent works(32). Because our model links integrin activation to mechanical stress, we propose to test further these differences by varying other parameters such as the width of the zone where the stress is applied.

These results are with respect the experimental findings of the first section. In our work, advanced lithography techniques allow to control the size of the adhesive spots at the cell-substrate contact interface. For this, we take the width w_0 as the typical size of the adhesive spots which thus corresponds in the model to the parts of the contact zone where the integrins are submitted to a stress. Although our model applies only at short time scales after the first contacts and integrin ligation, we propose that it serves as a template

to discuss more mature focal adhesion complexes which develop from these nascent adhesion clusters.

In short, by imposing a mechanical constraint, the model predicts different spatial organization for cell receptors which, thereby, may alter the specificity of their signaling functions. This hypothesis is explicit in the biological literature (33, 34) and a mark of our model is to define a framework from only three experimentally accessible quantities.

Acknowledgments

Appendix A

To find the local free energy per unit surface area, we work in the framework of a lattice gas model where each site can be occupied by an integrin of density n_0. Activated talin is free to diffuse on the membrane seen an adlayer and it can get reversibly adsorbed on the sites occupied by the integrins.

$$f(\phi_I, h) = \left(-A_I\phi_I + \frac{1}{2}k_b h(\mathbf{x})^2 \right) n_b(\phi_I, h) - A_I\phi_I n_u(\phi_I, h) \qquad (21)$$

To evaluate $\mu([\phi_I], h)$ as (8), we consider only the most singular term

$$n_0\Delta\mu(\phi_I, h) = \frac{1}{2}k_b h(\mathbf{x})^2 \left.\frac{\partial n_b}{\partial \phi_I}\right|_{\phi_I=\phi/K_m} - A_I n_0 \qquad (22)$$

Note that the derivative disappears if talin had a very high affinity for integrin, since n_b would not vary.

Introducing the rate of production ν_1 for activated talin, the equation of motion follows :

$$\frac{\partial\phi}{\partial t} = D\Delta\phi + \nu_1 - \gamma_1\phi - n_0k_{+1}\phi + n_0k_{-1,0}e^{\beta\Delta\mu(\phi_I,h)}\phi_I \qquad (23)$$

which together with Eq. (2) can be used to find the stationary solutions.

A convenient way to solve Eq. (23) is to introduce a reference state at zero stress $h(\mathbf{x}) = 0$. This reference state ϕ_0 is homogeneous and solves the equation of motion :

$$\nu_1 - \gamma_1\phi_0 - n_0k_{+1}\phi_0 + n_0k_{-1,0}e^{\beta\Delta\mu(\phi_{I,0},0)}\phi_{I,0} = 0 \qquad (24)$$

with the steady state condition Eq. (2) at zero stress. Thus ϕ_0 is an increasing function of the rate of ν_1 with which talin is activated by binding talin to the membrane with PIP_2. If this rate is large enough, as it is generally the case, since PIP_2 is produced at a very large rate, this state can used as a reference state.

Making the change of variable $\phi \to \phi_0 + \phi$, we look for a solution $\phi(\mathbf{x}, \mathbf{t})$ proportional to the rigidity k_b. To linear order, $e^{\beta\Delta\mu} \simeq 1 + \beta\Delta\mu$, since $\Delta\mu$ is linear in k_b. We find that the relative excess of concentration $\phi(\mathbf{x}, t)$ is

solution of the equation used in text

$$\frac{\partial \phi}{\partial t} = D\Delta\phi - b\phi + \frac{1}{2}\Gamma_I k_b h(\mathbf{x})^2 \frac{\partial n_b}{\partial \phi} \tag{25}$$

$$b = \gamma_1 + n_0 k_{+1} - n_0 k_{-1,0} \tag{26}$$

$$\Gamma_I = \beta^2 k_{-1} A_I \phi_{I,0} \tag{27}$$

$$\phi_{I,0} = \frac{k_{-1,0} + \gamma_2}{k_{+1}}\phi_0 \tag{28}$$

$$\frac{\partial n_b}{\partial \phi} = n_0 \frac{K_e^{0-1} e^{\beta\left(1/2 k_b h(\mathbf{x})^2 - A_I \phi\right)}}{\left[1 + K_e^{0-1} e^{\beta(1/2 k_b h(\mathbf{x})^2 - A_I \phi)}\right]^2} \tag{29}$$

with K_e^0 evaluated in the reference state at zero stress.

$$K_e^0 = K_{e,0} e^{\beta A_I \phi_{I,0}} \tag{30}$$

Note that to make this evolution equation as simple as possible, we have neglected terms $\phi \partial n_b / \partial \phi$ which are next order in k_b and saturate in the large ϕ limit by the condition Eq. (2). Finally, less singular contributions to the chemical potential such as $n_b(\phi, h)$ which appear when taking the derivative Eq. (8) will change the low ϕ limit of $f(\phi, h_0)$ in Figure 3 without affecting the bistable characteristic property.

Table

Symbol	Meaning	Typical value
k_b	Effective spring constant for integrin-substrate rigidity	0.3 mN.m^{-1}(35)
$1/b$	Effective residence time of talin	80-100 s (36, 37)
h_0	Range for the elastic strain	$1 - 15 \, nm$
D_n	Integrin Diffusion constant	$10^{-3} - 10^{-2} \mu m^2.s^{-1}$(38)
D_ϕ	Effective diffusion constant of PIP$_2$ bound talin	$0.2 \, \mu m^2.s^{-1}$(39)
n_∞	Averaged integrin density at zero stress	$100 - 500 \mu m^{-2}$(13)
l_0	Length of the extracellular domain of an integrin	$10 \, nm$(5, 40)
k_{-1}	Rate dissociation constant for the talin-integrin complex	$10^{-4} - 10^{-3} s^{-1}$(41)
A_I	Interaction energy between talin and integrin	$\simeq 10 - 20 k_B T$(42)
$A_I \phi_{I,0}$	Talin-integrin interaction energy at zero stress	$\simeq 1 - 5 k_B T$
K_e^0	$= n_b/n_0 = K_{e,0} e^{\beta A_I \phi_{I,0}}$ at zero stress	10^{-3}
K_m	Equivalent Michaelis-Menten constant for talin degradation	$\simeq 10^3 - 10^4 \mu m^{-2}$
$1/\beta$	$k_B T \simeq 4.1 \, pN.nm$	

Table 1: List of symbols with typical values used in this work.

References

1. Hynes, R. O. 2002. Integrins: bidirectional, allosteric signaling machines. *Cell.* 110:673–687.

2. Vogel, V., and M. Sheetz. 2006. Local force and geometry sensing regulate cell functions. *Nat Rev Mol Cell Biol.* 7:265–275.

3. Calderwood, D. A. 2004. Talin controls integrin activation. *Biochem Soc Trans.* 32:434–7.

4. Moser, M., K. R. Legate, R. Zent, and R. Fässler. 2009. The tail of integrins, talin, and kindlins. *Science.* 324:895–9.

5. Shattil, S. J., C. Kim, and M. H. Ginsberg. 2010. The final steps of integrin activation: the end game. *Nat Rev Mol Cell Biol.* 11:288–300.

6. Anthis, N. J., and I. D. Campbell. 2011. The tail of integrin activation. *Trends Biochem Sci.* .

7. Cluzel, C., F. Saltel, J. Lussi, F. Paulhe, B. A. Imhof, and B. Wehrle-Haller. 2005. The mechanisms and dynamics of (alpha)v(beta)3 integrin clustering in living cells. *J Cell Biol.* 171:383–92.

8. Bouaouina, M., Y. Lad, and D. A. Calderwood. 2008. The n-terminal domains of talin cooperate with the phosphotyrosine binding-like domain to activate beta1 and beta3 integrins. *J Biol Chem.* 283:6118–25.

9. Calderwood, D. A., B. Yan, J. M. de Pereda, B. G. Alvarez, Y. Fujioka, R. C. Liddington, and M. H. Ginsberg. 2002. The phosphotyrosine binding-like domain of talin activates integrins. *J Biol Chem.* 277:21749–58.

10. Anthis, N. J., K. L. Wegener, F. Ye, C. Kim, B. T. Goult, E. D. Lowe, I. Vakonakis, N. Bate, D. R. Critchley, M. H. Ginsberg, and I. D. Campbell. 2009. The structure of an integrin/talin complex reveals the basis of inside-out signal transduction. *EMBO J.* 28:3623–32.

11. Ye, F., G. Hu, D. Taylor, B. Ratnikov, A. A. Bobkov, M. A. McLean, S. G. Sligar, K. A. Taylor, and M. H. Ginsberg. 2010. Recreation of the terminal events in physiological integrin activation. *J Cell Biol.* 188:157–73.

12. Streicher, P., P. Nassoy, M. Bärmann, A. Dif, V. Marchi-Artzner, F. Brochard-Wyart, J. Spatz, and P. Bassereau. 2009. Integrin reconstituted in guvs: a biomimetic system to study initial steps of cell spreading. *Biochim Biophys Acta*. 1788:2291–300.

13. Wiseman, P. W., C. M. Brown, D. J. Webb, B. Hebert, N. L. Johnson, J. A. Squier, M. H. Ellisman, and A. F. Horwitz. 2004. Spatial mapping of integrin interactions and dynamics during cell migration by image correlation microscopy. *J Cell Sci*. 117:5521–34.

14. Bershadsky, A., M. Kozlov, and B. Geiger. 2006. Adhesion-mediated mechanosensitivity: a time to experiment, and a time to theorize. *Curr Opin Cell Biol*. 18:472–481.

15. Bruinsma, R. 2005. Theory of force regulation by nascent adhesion sites. *Biophys J*. 89:87–94.

16. Nicolas, A., B. Geiger, and S. A. Safran. 2004. Cell mechanosensitivity controls the anisotropy of focal adhesions. *Proc Natl Acad Sci U S A*. 101:12520–12525.

17. Nicolas, A., A. Besser, and S. A. Safran. 2008 Jul. Dynamics of cellular focal adhesions on deformable substrates: consequences for cell force microscopy. *Biophys J*. 95:527–539.

18. Besser, A., and S. A. Safran. 2006. Force-induced adsorption and anisotropic growth of focal adhesions. *Biophys J*. 90:3469–84.

19. Novak, I. L., B. M. Slepchenko, A. Mogilner, and L. M. Loew. 2004. Cooperativity between cell contractility and adhesion. *Phys Rev Lett*. 93:268109.

20. Guillou, H., A. Depraz-Depland, E. Planus, B. Vianay, J. Chaussy, A. Grichine, C. Albiges-Rizo, and M. R. Block. 2008 Feb 1. Lamellipodia nucleation by filopodia depends on integrin occupancy and downstream rac1 signaling. *Exp Cell Res*. 314:478–488.

21. Vianay, B., J. Käfer, E. Planus, M. Block, F. Graner, and H. Guillou. 2010. Single cells spreading on a protein lattice adopt an energy minimizing shape. *Phys Rev Lett*. 105:128101.

22. Martel, V., C. Racaud-Sultan, S. Dupe, C. Marie, F. Paulhe, A. Galmiche, M. R. Block, and C. Albiges-Rizo. 2001. Conformation, localization, and integrin binding of talin depend on its interaction with phosphoinositides. *J Biol Chem.* 276:21217–21227.

23. Harburger, D. S., M. Bouaouina, and D. A. Calderwood. 2009. Kindlin-1 and -2 directly bind the c-terminal region of beta integrin cytoplasmic tails and exert integrin-specific activation effects. *J Biol Chem.* 284:11485–97.

24. Huang, C., Z. Rajfur, N. Yousefi, Z. Chen, K. Jacobson, and M. H. Ginsberg. 2009. Talin phosphorylation by cdk5 regulates smurf1-mediated talin head ubiquitylation and cell migration. *Nat Cell Biol.* 11:624–30.

25. Yan, B., D. A. Calderwood, B. Yaspan, and M. H. Ginsberg. 2001. Calpain cleavage promotes talin binding to the beta 3 integrin cytoplasmic domain. *J Biol Chem.* 276:28164–70.

26. Bell, G. I., M. Dembo, and P. Bongrand. 1984. Cell adhesion. competition between nonspecific repulsion and specific bonding. *Biophys J.* 45:1051–64.

27. Ward, M. D., M. Dembo, and D. A. Hammer. 1994. Kinetics of cell detachment : Peeling of discrete receptor clusters. *Biophys. J.* 67:2522–2534.

28. Munevar, S., Y. Wang, and M. Dembo. 2004. Regulation of mechanical interactions between fibroblast and substratum by strech-activated ca2+ entry. *J. Cell Science.* 117:85–92.

29. Li, F., S. D. Redick, H. P. Erickson, and V. T. Moy. 2003. Force measurements of the alpha5beta1 integrin-fibronectin interaction. *Biophys J.* 84:1252–62.

30. Ali, O., C. Albigès-Rizo, M. R. Block, and B. Fourcade. 2009. Excitable waves at the margin of the contact area between a cell and a substrate. *Phys Biol.* 6:25010.

31. Wang, Y., E. L. Botvinick, Y. Zhao, M. W. Berns, S. Usami, R. Y. Tsien, and S. Chien. 2005 Apr 21. Visualizing the mechanical activation of src. *Nature.* 434:1040–1045.

32. Roca-Cusachs, P., N. C. Gauthier, A. Del Rio, and M. P. Sheetz. 2009. Clustering of alpha(5)beta(1) integrins determines adhesion strength whereas alpha(v)beta(3) and talin enable mechanotransduction. *Proc Natl Acad Sci U S A*. 106:16245–50.

33. Paszek, M., and V. Weaver. 2010. Biophysics. enforcing order on signaling. *Science*. 327:1335–6.

34. Salaita, K., P. M. Nair, R. S. Petit, R. M. Neve, D. Das, J. W. Gray, and J. T. Groves. 2010. Restriction of receptor movement alters cellular response: physical force sensing by epha2. *Science*. 327:1380–5.

35. Taubenberger, A., D. A. Cisneros, J. Friedrichs, P.-H. Puech, D. J. Muller, and C. M. Franz. 2007. Revealing early steps of alpha2beta1 integrin-mediated adhesion to collagen type i by using single-cell force spectroscopy. *Mol Biol Cell*. 18:1634–1644.

36. Himmel, M., A. Ritter, S. Rothemund, B. V. Pauling, K. Rottner, A. R. Gingras, and W. H. Ziegler. 2009. Control of high affinity interactions in the talin c terminus: how talin domains coordinate protein dynamics in cell adhesions. *J Biol Chem*. 284:13832–42.

37. Lele, T. P., C. K. Thodeti, J. Pendse, and D. E. Ingber. 2008. Investigating complexity of protein-protein interactions in focal adhesions. *Biochem Biophys Res Commun*. 369:929–34.

38. Duband, J. L., G. H. Nuckolls, A. Ishihara, T. Hasegawa, K. M. Yamada, J. P. Thiery, and K. Jacobson. 1988. Fibronectin receptor exhibits high lateral mobility in embryonic locomoting cells but is immobile in focal contacts and fibrillar streaks in stationary cells. *J Cell Biol*. 107:1385–96.

39. Golebiewska, U., M. Nyako, W. Woturski, I. Zaitseva, and S. McLaughlin. 2008. Diffusion coefficient of fluorescent phosphatidylinositol 4,5-bisphosphate in the plasma membrane of cells. *Mol Biol Cell*. 19:1663–9.

40. Takagi, J., H. P. Erickson, and T. A. Springer. 2001. C-terminal opening mimics 'inside-out' activation of integrin alpha5beta1. *Nat Struct Biol*. 8:412–6.

41. Yan, B., D. A. Calderwood, B. Yaspan, and M. H. Ginsberg. 2001. Calpain cleavage promotes talin binding to the beta 3 integrin cytoplasmic domain. *J Biol Chem.* 2001:10.1074/jbc.M104161200.

42. Anthis, N. J., K. L. Wegener, D. R. Critchley, and I. D. Campbell. 2010. Structural diversity in integrin/talin interactions. *Structure.* 18:1654–66.

43. Critchley, D. R. 2004. Cytoskeletal proteins talin and vinculin in integrin-mediated adhesion. *Biochem Soc Trans.* 32:831–6.

44. Abramowitz, M., and I. Stegun. 1972. Handbook of Mathematical Functions. National Bureau of Standards.

Figure Legends

Figure 1.

Fibroblasts adhering on fibronectin patterned substrates. The left panel corresponds to cells adhering to $4 \times 4 \, \mu m$ fibronectin plots and the right panel to $2 \times 2 \, \mu m$ plots. Adhesive plots are visualized by alexa350 labeled fibronectin, actin filaments are labeled with TRIRC phalloïdin and focal adhesion by a monoclonal anti vinculin antibody and a Alexa488 labeled secondary antibody (see supplemental section). For the largest plots the focal adhesion complexes split into two parts with two stress fibers connecting opposite plots. For the smallest plots, however, the focal adhesive clusters appear homogeneous with only one stress fiber emerging from the adhesion complexes. The transition from one to two adhesive spots on the same plot is geometry independent since all cells adhering to square or triangular lattices exhibit the same behavior.

Figure 2.

Schematic view of the talin activation cycle (after (43)). (1) Talin in its inactivated state (ϕ_c) in the cytosol. Talin is recruted at the membrane (ϕ_m) and is activated by binding to PIP_2. In this activated state, ϕ, talin interacts with the integrins (step 3). The equilibrium between activated talin ϕ and the integrin (the bound complex is denoted ϕ_I) is crucial. In (4), talin unbinds from the integrin and goes back to its cytosolic state (ϕ_c).

Figure 3

Plot of the effective source function $f(\phi, h_0)$ as a function of ϕ for different values of h_0. The figure shows $f(\phi, h_0)$ for four different values of the strain index h_0. The dotted and dashed lines are for $h_0 < h_{c_1}$. For $h_0 > h_{c_1}$, $f(\phi, h_0)$ has three roots instead of one. The "shark" teeth shaped curve corresponds to the β_∞ approximation as taken in the text when passing from Eq. (15) to Eq. (17). Finally, the last curve for $h_{c_2} < h_0$ corresponds to the nearly saturated regime where $\phi_I = \phi/(K_m + \phi)$ instead of $\phi_I = \phi/K_m$ as in the three previous plots. In this case, the source function $f(\phi, h_0)$ has only one zero for some value of $h(x_0)$.

Figure 4

(a) Plot of the type 1 family talin concentration $A_I\phi_1(w_0x)/K_m$ for parameter values taken from Table 1. The dashed curve is the approximate analytical solution with $c = 0$ (see the supplemental data section). Otherwise, numerical solutions and thick curves corresponding to type 1 solutions of the β_∞ model coincide on the scale of the figure. Finally, the thin curve corresponds to the asymptotic expansion of the analytical solution given by Eq. (**??**). It shows that asymptotic results are already reliable even if $\sqrt{D/b} = 0.28w_0$ as in the case of this figure. Color code indicates that $1/2\beta k_b h_0^2$ decreases stepwise (15, 7.5, 4.5 to 3) with the largest value in green. (b) Plot of the type 2 family solutions $A_I\phi_2(w_0x)/K_m$. Dashed curves correspond to numerical solutions. Thick and dashed curves coincide when $\phi_3^\star$ goes to zero smoothly as $|x|$ goes to infinity. Plain circles correspond to the boundary points x_0 for type 2 solutions where the solution passes through the singularity of the β_∞ model. Decreasing h_0 changes the solution till it matches a type 1 solution at the bifurcation point. The color code for Fig. 4-b is the same as for Fig. 4-a. (c) Plot of the density of engaged integrin $n_b(w_0x)$ for centered type 1 and type 2 solutions for the same parameters $(1/2\beta k_b h_0^2 = 4.5)$. For convenience, type 1 solutions have been scaled down by a factor 10 $(w_0 = 10\mu m)$.

Figure 5

(a) Plot of of the talin density $A_I\phi(w_0x)/K_m$ as a function of x. Decreasing the ratio w_0/λ at fixed strain h_0 decreases the characteristic distance between the two maxima. Decreasing this ratio further leads to a critical width where type 2 solutions stop existing. For $w_0 < w_c$, the only solution is of type 1 and corresponds to the centered distribution shown in the Figure. (b) Plot of $n_b(w_0x)/n_\infty$. Although $A_I\phi_1(w_0x)/K_m$ is always maximum at the origin, $n_b(x)$ for type 1 solution can be minimum in the near vicinity of the bifurcation point. In both figures, $w_c \simeq 2.5\mu m$ (for both figures, $\lambda \simeq 2.8\mu m$ and the color code indicates that w_0 decreases in steps of $1\,\mu m$ from 6 to $2\mu m$).
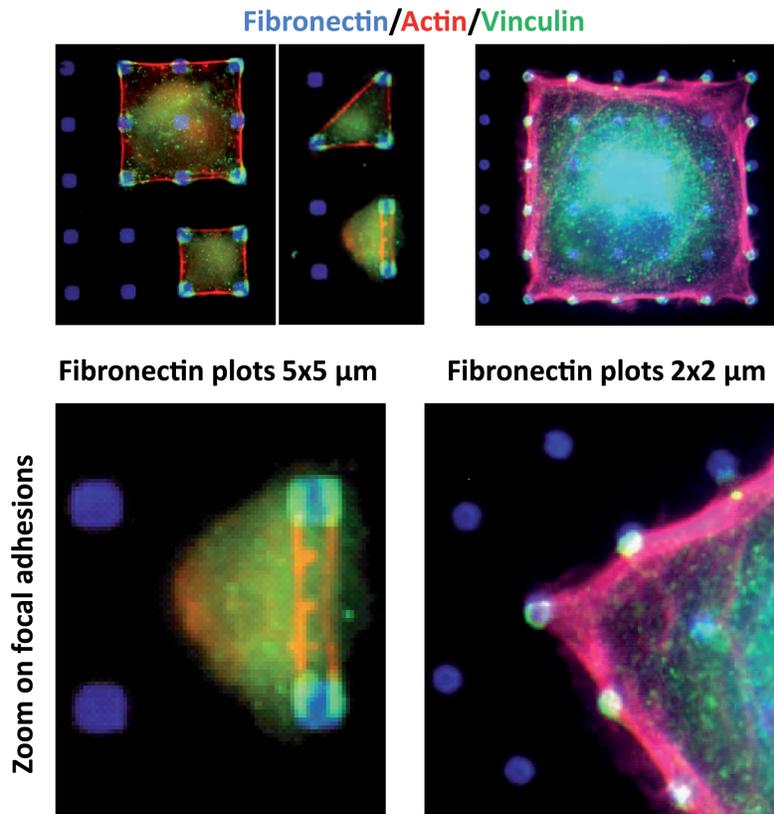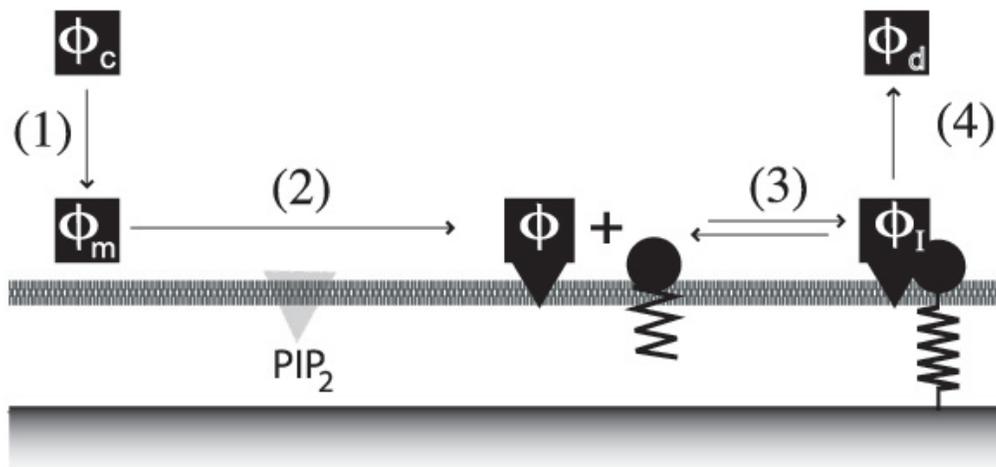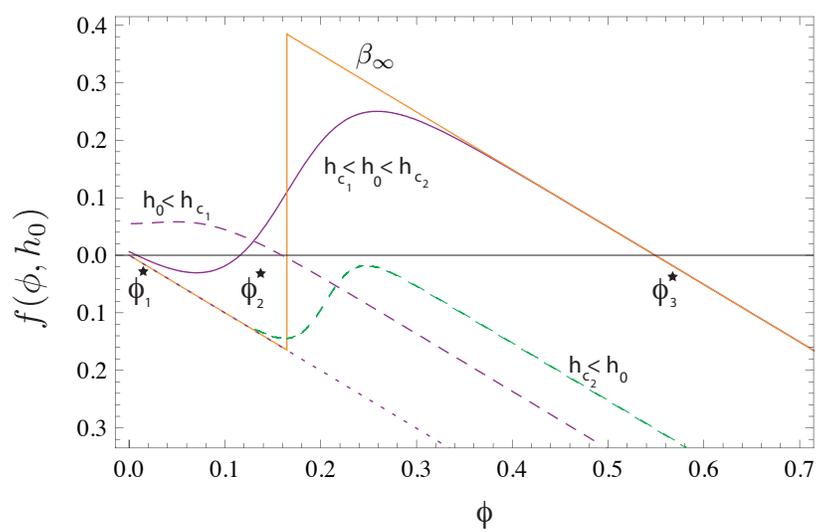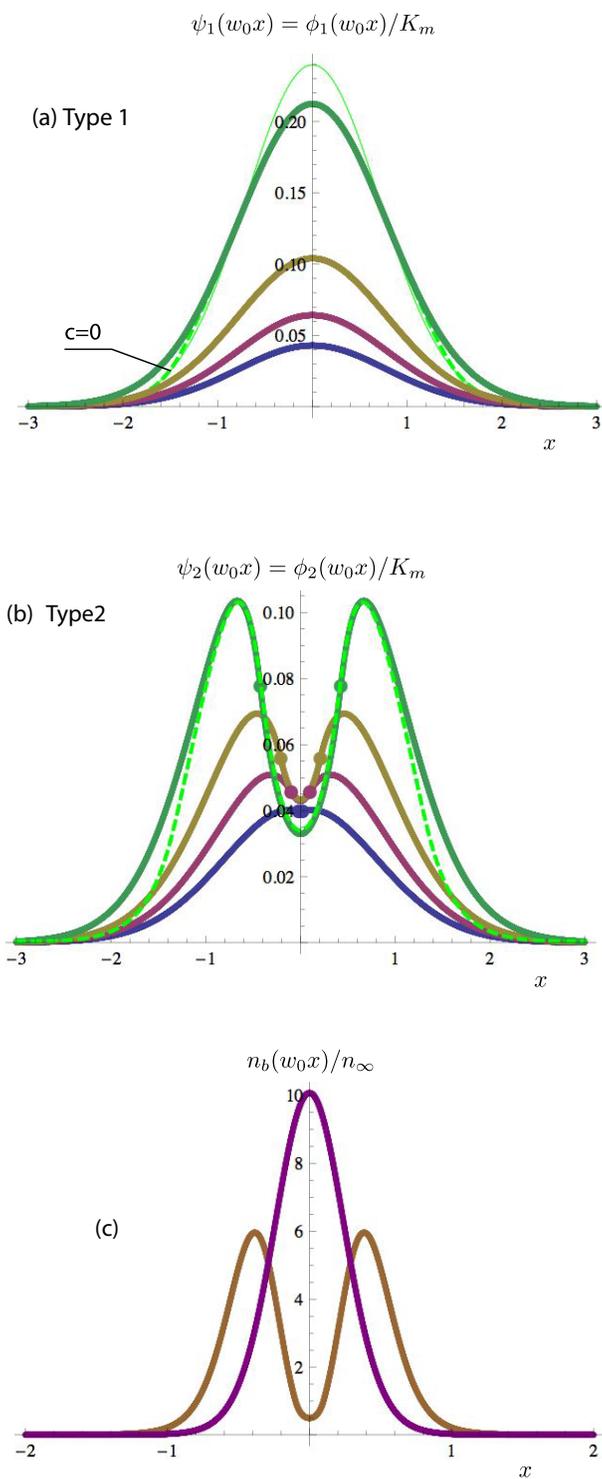
Figure 1:

Figure 2:

Figure 3:

$$\psi_1(w_0 x) = \phi_1(w_0 x)/K_m$$

(a) Type 1

c=0

x

$$\psi_2(w_0 x) = \phi_2(w_0 x)/K_m$$

(b) Type2

x

$$n_b(w_0 x)/n_\infty$$

(c)

x

Figure 4:

(a) $\psi_1(x) = \phi_1(x)/K_m$

Type 1 : $w_0 < w_c$

Type 2 : $w_0 > w_c$

(b) $n_b(x)/n_\infty$

Type 1 : $w_0 < w_c$
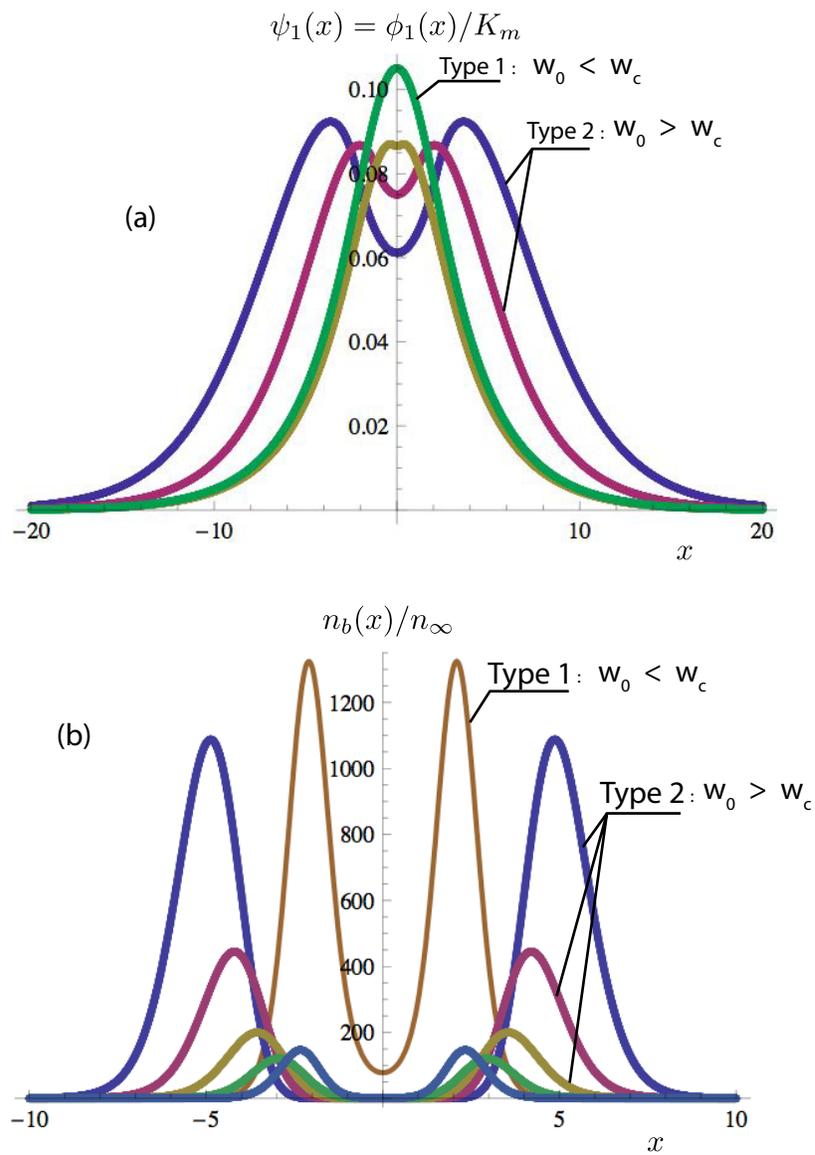
Type 2 : $w_0 > w_c$

Figure 5:

Appendix A

To find the local free energy per unit surface area, we work in the framework of a lattice gas model where each site can be occupied by an integrin of density n_0. Activated talin is free to diffuse on the membrane seen an adlayer and it can get reversibly adsorbed on the sites occupied by the integrins.

$$f(\phi_I, h) = \left(-A_I\phi_I + \frac{1}{2}k_b h(\mathbf{x})^2\right) n_b(\phi_I, h) - A_I\phi_I n_u(\phi_I, h) \qquad (21)$$

To evaluate $\mu([\phi_I], h)$ as (8), we consider only the most singular term

$$n_0\Delta\mu(\phi_I, h) = \frac{1}{2}k_b h(\mathbf{x})^2 \left.\frac{\partial n_b}{\partial \phi_I}\right|_{\phi_I=\phi/K_m} - A_I n_0 \qquad (22)$$

Note that the derivative disappears if talin had a very high affinity for integrin, since n_b would not vary.

Introducing the rate of production ν_1 for activated talin, the equation of motion follows :

$$\frac{\partial\phi}{\partial t} = D\Delta\phi + \nu_1 - \gamma_1\phi - n_0 k_{+1}\phi + n_0 k_{-1,0} e^{\beta\Delta\mu(\phi_I,h)}\phi_I \qquad (23)$$

which together with Eq. (2) can be used to find the stationary solutions.

A convenient way to solve Eq. (23) is to introduce a reference state at zero stress $h(\mathbf{x}) = 0$. This reference state ϕ_0 is homogeneous and solves the equation of motion :

$$\nu_1 - \gamma_1\phi_0 - n_0 k_{+1}\phi_0 + n_0 k_{-1,0} e^{\beta\Delta\mu(\phi_{I,0},0)}\phi_{I,0} = 0 \qquad (24)$$

with the steady state condition Eq. (2) at zero stress. Thus ϕ_0 is an increasing function of the rate of ν_1 with which talin is activated by binding talin to the membrane with PIP_2. If this rate is large enough, as it is generally the case, since PIP_2 is produced at a very large rate, this state can used as a reference state.

Making the change of variable $\phi \to \phi_0 + \phi$, we look for a solution $\phi(\mathbf{x}, \mathbf{t})$ proportional to the rigidity k_b. To linear order, $e^{\beta\Delta\mu} \simeq 1 + \beta\Delta\mu$, since $\Delta\mu$ is linear in k_b. We find that the relative excess of concentration $\phi(\mathbf{x}, t)$ is

solution of the equation used in text

$$\frac{\partial \phi}{\partial t} = D\Delta\phi - b\phi + \frac{1}{2}\Gamma_I k_b h(\mathbf{x})^2 \frac{\partial n_b}{\partial \phi} \tag{25}$$

$$b = \gamma_1 + n_0 k_{+1} - n_0 k_{-1,0} \tag{26}$$

$$\Gamma_I = \beta^2 k_{-1} A_I \phi_{I,0} \tag{27}$$

$$\phi_{I,0} = \frac{k_{-1,0} + \gamma_2}{k_{+1}}\phi_0 \tag{28}$$

$$\frac{\partial n_b}{\partial \phi} = n_0 \frac{K_e^{0-1} e^{\beta\left(1/2k_b h(\mathbf{x})^2 - A_I\phi\right)}}{\left[1 + K_e^{0-1} e^{\beta(1/2k_b h(\mathbf{x})^2 - A_I\phi)}\right]^2} \tag{29}$$

with K_e^0 evaluated in the reference state at zero stress.

$$K_e^0 = K_{e,0} e^{\beta A_I \phi_{I,0}} \tag{30}$$

Note that to make this evolution equation as simple as possible, we have neglected terms $\phi \partial n_b/\partial \phi$ which are next order in k_b and saturate in the large ϕ limit by the condition Eq. (2). Finally, less singular contributions to the chemical potential such as $n_b(\phi, h)$ which appear when taking the derivative Eq. (8) will change the low ϕ limit of $f(\phi, h_0)$ in Figure 3 without affecting the bistable characteristic property.

Table

Symbol	Meaning	Typical value
k_b	Effective spring constant for integrin-substrate rigidity	0.3 mN.m^{-1}(35)
$1/b$	Effective residence time of talin	80-100 s (36, 37)
h_0	Range for the elastic strain	$1-15\,nm$
D_n	Integrin Diffusion constant	$10^{-3}-10^{-2}\mu m^2.s^{-1}$(38
D_ϕ	Effective diffusion constant of PIP$_2$ bound talin	$0.2\,\mu m^2.s^{-1}$(39)
n_∞	Averaged integrin density at zero stress	$100-500\mu m^{-2}$(13)
l_0	Length of the extracellular domain of an integrin	$10\,nm$(5, 40)
k_{-1}	Rate dissociation constant for the talin-integrin complex	$10^{-4}-10^{-3}s^{-1}$(41)
A_I	Interaction energy between talin and integrin	$\simeq 10-20k_BT$(42)
$A_I\phi_{I,0}$	Talin-integrin interaction energy at zero stress	$\simeq 1-5k_BT$
K_e^0	$= n_b/n_0 = K_{e,0}e^{\beta A_I\phi_{I,0}}$ at zero stress	10^{-3}
K_m	Equivalent Michaelis-Menten constant for talin degradation	$\simeq 10^3-10^4\mu m^{-2}$
$1/\beta$	$k_BT \simeq 4.1\,pN.nm$	

Table 1: List of symbols with typical values used in this work.